

# Inherently Selective Water-Free Deposition of Titanium Dioxide on the Nanoscale: Implications for Nanoscale Patterning

Yunil Cho, Christopher F. Ahles, Jong Youn Choi, James Huang, Antony Jan, Keith Wong, Srinivas Nemani, Ellie Yieh, and Andrew C. Kummel\*



Cite This: *ACS Appl. Nano Mater.* 2022, 5, 476–485



Read Online

ACCESS |



Metrics & More

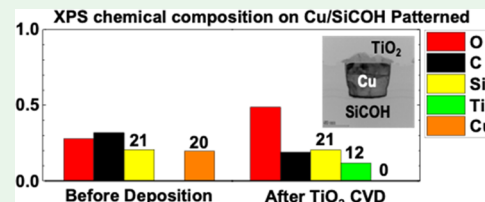


Article Recommendations



Supporting Information

**ABSTRACT:** Water-free inherent selective deposition of TiO<sub>2</sub> on Si and SiO<sub>2</sub> in preference to SiCOH has been studied via atomic layer deposition (ALD) and pulsed chemical vapor deposition (CVD). SiCOH is a nonreactive low-*k* dielectric material, consisting of highly porous alkylated SiO<sub>2</sub>. Water-free deposition was studied to protect SiCOH and increase selectivity. The titanium precursor used in all studies was Ti(O<sup>i</sup>Pr)<sub>4</sub> [titanium(IV) isopropoxide] and contains four oxygen atoms enabling it to form TiO<sub>2</sub> through single-precursor CVD. At 250 °C substrate temperature, selective water-free ALD of TiO<sub>2</sub> using Ti(O<sup>i</sup>Pr)<sub>4</sub> and either acetic acid (AcOH) or formic acid (HCO<sub>2</sub>H) as a second precursor was studied. By both ALD processes, around 2 nm of TiO<sub>2</sub> was deposited on Si and SiO<sub>2</sub> without any deposition on SiCOH. The TiO<sub>2</sub> ALD films had a root-mean-square roughness of 2–3 Å. *In situ* X-ray photoelectron spectroscopy showed that Ti(O<sup>i</sup>Pr)<sub>4</sub> + AcOH ALD occurred via ligand exchange between –O<sup>i</sup>Pr and AcO–. ALD with formic acid, which is a 10× stronger proton donor than acetic acid, displayed similar selectivity but with a 10× higher growth rate than ALD with acetic acid. Single-precursor pulsed CVD with Ti(O<sup>i</sup>Pr)<sub>4</sub> was also studied at 250 and 295 °C substrate temperatures. At 250 °C, TiO<sub>2</sub> growth on all substrates was minuscule (<1 nm for 400 pulses). Single-precursor pulsed CVD (2000 pulses) at 295 °C displayed the highest selectivity among all processes studied: 16.9 and 40.1 nm TiO<sub>2</sub> molecules were deposited on Si and SiO<sub>2</sub>, respectively, while less than a monolayer of TiO<sub>2</sub> was deposited on SiCOH. The pulsed CVD at 295 °C showed ~20 nm of selective TiO<sub>2</sub> deposition on nanoscale patterned samples. It is expected that the selective TiO<sub>2</sub> CVD can be applicable in the nanoscale patterning process in metal-oxide-semiconductor field-effect transistor fabrication.



**KEYWORDS:** inherent selective deposition, selective oxide deposition, water-free deposition, nanoscale patterning, titanium oxide

## 1. INTRODUCTION

Atomic layer deposition (ALD) and chemical vapor deposition (CVD) are widely used techniques in the semiconductor industry. ALD uses self-limiting chemical reactions in which an oxidant (e.g., H<sub>2</sub>O) and a reductant (typically an organometallic precursor) are pulsed into a vacuum chamber containing the substrate in succession (half cycles); in each half cycle, ligand exchange occurs between surface species and gaseous precursor species. Thermal CVD is typically performed using oxidizing and reducing precursors that are continuously and simultaneously dosed into a chamber containing the substrate at a higher sample temperature than ALD. The increased surface temperature results in the decomposition of the precursors and the reaction to form a thermodynamically favorable material. For CVD of oxide materials, this leaves a highly reactive surface terminated by hydroxyl (–OH) groups, which then react with further precursors to quickly deposit the material of interest.<sup>1</sup> While ALD is self-limiting in reaction progression and typically forms smooth and conformal films, CVD dosing conditions must be carefully controlled to produce smooth and conformal films.<sup>2</sup>

ALD and CVD methods have been used in the semiconductor industry,<sup>3</sup> and selective deposition may enable their

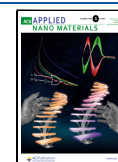
use in nanoscale fabrication.<sup>4</sup> For example, selective oxide deposition can be integrated into patterning methods such as spacer-defined double patterning (SDDP). This method can reduce the mask misalignment issue during metal-oxide-semiconductor field-effect transistor (MOSFET) scaling.<sup>5,6</sup> Conventional nonselective ALD and CVD can also be employed in SDDP; however, selective deposition reduces the number of process steps (etch spacer step), as shown in Figure 1, which can reduce cost and time.

Three selective deposition methods can be used: inherent selective deposition, selective passivation, and selective activation. Inherent selective deposition is based on the reactivity difference for precursor-mediated chemisorption of one or both precursors on different surfaces. This method is most desirable because it requires only one step for the selective deposition; however, only limited research has been

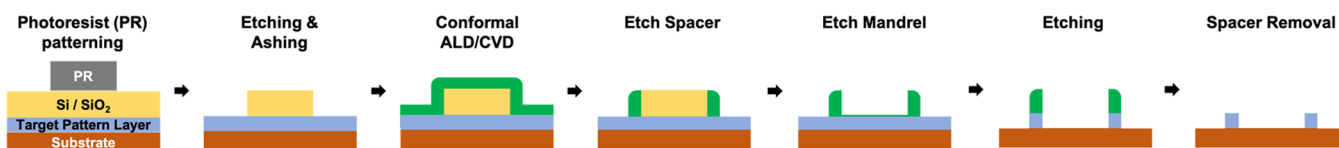
**Received:** October 8, 2021

**Accepted:** January 5, 2022

**Published:** January 19, 2022



## 1) Spacer Defined Double Patterning with conventional ALD/CVD



## 2) Spacer Defined Double Patterning with selective ALD/CVD

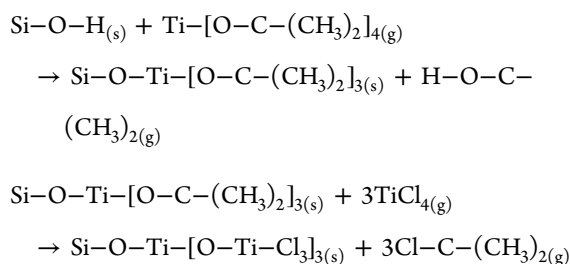


**Figure 1.** Schematic showing the process for SDDP with (1) conventional ALD/CVD and (2) selective ALD/CVD. Selective oxide deposition enables a reduction in the number of process steps (etch spacer step).

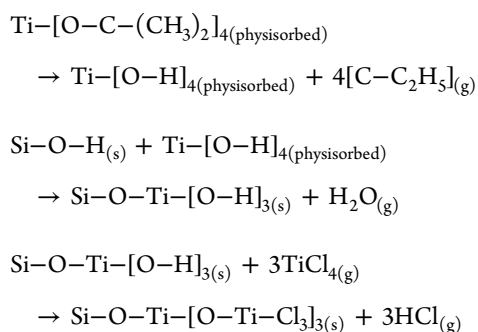
reported.<sup>7–10</sup> The majority of current selective depositions rely on selective passivation, where a molecule, such as long-chain alkane, selectively reacts on a specific surface and prevents any deposition on that surface.<sup>11–15</sup> Selective activation, which induces deposition only on the surface with certain pretreatments (e.g., electron beam-induced deposition), has also been reported.<sup>16–19</sup>

For high-selectivity oxide deposition, it is preferred to have an oxygen source other than water ( $\text{H}_2\text{O}$ ), for example, a metal alkoxide precursor or a carboxylic acid, since water can react on almost any surface and induce oxidation. There have been many reports of  $\text{TiO}_2$  deposition via ALD and CVD including water-free ALD of  $\text{TiO}_2$  using  $\text{Ti}(\text{O}^i\text{Pr})_4$  and  $\text{TiCl}_4$ .<sup>1,20,21</sup> There are two mechanisms for the combination of these two precursors, depending on the sample temperature.<sup>21</sup> The chemical equations for each mechanism are shown below.

## 1 Low temperature (125–225 °C)



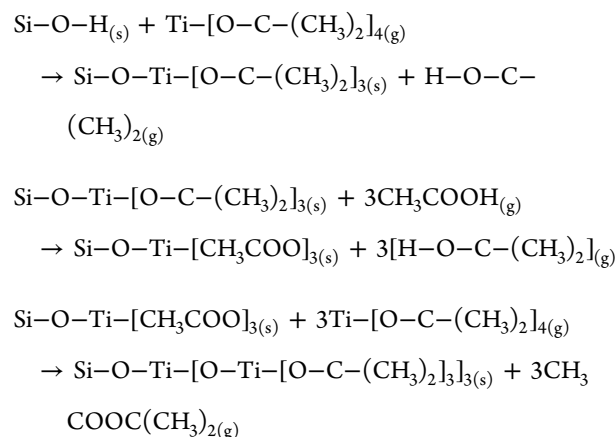
## 2 High temperature (250–300 °C)



At low temperatures (125–225 °C),  $\text{Ti}(\text{O}^i\text{Pr})_4$  reacts on the surface and produces  $\text{Ti-O-}^i\text{Pr}$  adsorbates. Sequentially dosed  $\text{TiCl}_4$  reacts with this  $\text{-O-}^i\text{Pr}$  ligand on the surface and produces  $\text{Ti-O-Ti}$  bonds. Conversely, at high temperatures (250–300 °C), the  $\text{Ti-O-}^i\text{Pr}$  bonds on the

physisorbed  $\text{Ti}(\text{O}^i\text{Pr})_4$  thermally decompose and form hydroxyl ligands ( $\text{Ti-OH}$  bonds). The hydroxyl ligands react with subsequent  $\text{TiCl}_4$  to produce  $\text{Ti-O-Ti}$  bonds. To summarize the reaction mechanism at high/low temperature, the ALD reaction is dominated at low temperature, but at high temperature, the reaction is a mixture of thermal CVD and ALD. The drawback of this process is that halogens, for example, Cl, can corrode metals, so that this process is incompatible with middle or back of the line processing.

Water-free  $\text{TiO}_2$  ALD using  $\text{Ti}(\text{O}^i\text{Pr})_4$  and  $\text{AcOH}$  was also reported with the mechanism given below.<sup>22</sup>



In this previous study,  $\text{Ti}(\text{O}^i\text{Pr})_4$  reacts on the  $\text{Si-OH}$  surface and produces  $\text{Ti-O-}^i\text{Pr}$  adsorbates at 200 °C. Subsequently dosed  $\text{CH}_3\text{COOH}$  ( $\text{AcOH}$ ) performs a ligand exchange reaction with the  $\text{-O-}^i\text{Pr}$  ligand on the surface and produces  $\text{Ti-OAc}$  bonds. This  $\text{Ti-OAc}$  then further reacts with  $\text{Ti}(\text{O}^i\text{Pr})_4$  and forms  $\text{Ti-O-Ti-O-}^i\text{Pr}$  bonds; subsequent ALD cycles deposit  $\text{TiO}_2$  films. These processes do not use  $\text{H}_2\text{O}$  as a second precursor, which protects low- $k$  dielectrics ( $\text{SiCOH}$ ) and increases the probability of selective deposition; however, selective deposition was not reported.

In the present study, water-free inherent selective ALD and CVD of  $\text{TiO}_2$  using  $\text{Ti}(\text{O}^i\text{Pr})_4$  and  $\text{HCO}_2\text{H}$  or  $\text{AcOH}$  on  $\text{Si}$ ,  $\text{SiO}_2$ , and  $\text{SiCOH}$  were investigated.  $\text{Ti}(\text{O}^i\text{Pr})_4$  is a metal alkoxide precursor which contains oxygen atoms in each ligand, so that this precursor can not only be used in ALD reactions but also be employed for unimolecular thermal CVD.  $\text{HCO}_2\text{H}$  and  $\text{AcOH}$  are the second precursors for the ALD reaction.  $\text{SiCOH}$ , which is alkylated porous  $\text{SiO}_2$ , has  $\text{Si-OC}_x\text{H}_y$  or  $\text{Si-C}_x\text{H}_y$  groups on the surface and does not contain

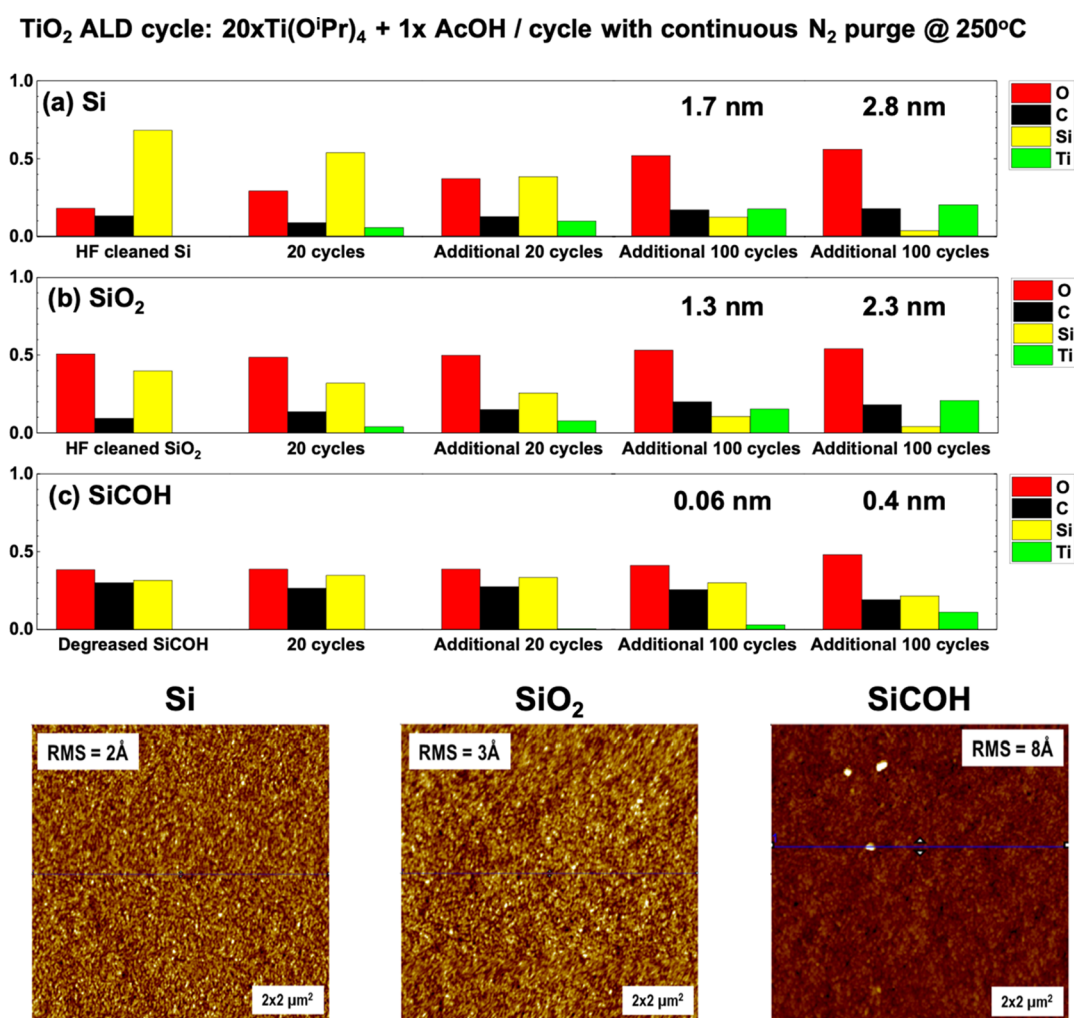


**Figure 2.** XPS chemical composition (above) and AFM image (below) of TiO<sub>2</sub> films after a total of 240 ALD cycles of Ti(O<sup>i</sup>Pr)<sub>4</sub> and AcOH at 250 °C. (a) On HF-etched Si: 2.8 nm of TiO<sub>2</sub> was deposited and the film was smooth with an rms roughness of 2 Å. (b) On HF-etched SiO<sub>2</sub>: 2.3 nm of TiO<sub>2</sub> was deposited and the film was smooth with an rms roughness of 3 Å. (c) On degreased SiCOH: ~0.4 nm of TiO<sub>2</sub> was deposited (calculated based on the attenuation of the Si substrate signal), and the surface rms roughness was 8 Å with several ~6 nm particles which were present on the SiCOH surface prior to deposition.

reactive sites such as –OH groups. Therefore, SiCOH in this sample set was used as the nonreactive surface.<sup>23–26</sup>

ALD reactions with both second precursors were performed at 250 °C substrate temperature. Both ALD reactions showed ~2 nm of smooth [2–3 Å root-mean-square (rms) roughness] TiO<sub>2</sub> deposition on Si and SiO<sub>2</sub> before appreciable deposition (~0.4 nm) was observed on SiCOH. The single-precursor pulsed CVD at 295 °C showed even higher selectivity with ~17 and ~40 nm films of TiO<sub>2</sub> on Si and SiO<sub>2</sub>, respectively. With ~20 nm of selective deposition on the nanoscale region, the pulsed CVD process showed its potential in nanoscale semiconductor fabrication, such as nanoscale patterning by merging with SDDP. However, high roughness (>1 nm rms roughness) due to the presence of nanocrystalline grains on the surface needs to be resolved for its application in nanoscale patterning using known techniques such as nanolaminate formation.<sup>27,28</sup>

## 2. EXPERIMENTAL SECTION

In the present study, selective ALD and CVD were tested on three different substrates: Si, SiO<sub>2</sub>, and SiCOH. Each substrate was diced and degreased with acetone, methanol, and deionized water for 15 s.

To remove the surface native oxide, degreased Si and SiO<sub>2</sub> substrates were immersed in a 0.5% hydrofluoric acid solution for 30 s. After the cleaning process, substrates were loaded to the ultrahigh vacuum (UHV) chamber on a single sample holder to go through the same dosing process.

Patterned Cu on SiCOH substrates was used to examine selective deposition in nanoscale features. These substrates were degreased using the process previously described. Since the SiCOH region of the patterned sample was damaged from the initial fabrication process and, therefore, not fully terminated with –OC<sub>x</sub>H<sub>y</sub> or –C<sub>x</sub>H<sub>y</sub> groups, an additional passivation was performed with a proprietary passivation process from Applied Materials.

ALD and CVD were performed in a home-made reaction chamber. The precursor dosing was controlled by pneumatic valves, and no carrier gas was used. Each precursor was transferred to a glass precursor bottle and connected to the chamber. The Ti(O<sup>i</sup>Pr)<sub>4</sub> bottle was heated up to 80 °C, while the AcOH and HCO<sub>2</sub>H bottles were kept at room temperature (~21 °C). A constant N<sub>2</sub> purge was used to evacuate the residual precursor from the chamber. All of the precursor dosings were controlled with the pressure inside the reaction chamber. The constant N<sub>2</sub> purge was controlled by a needle valve, and the pressure size of the precursor pulse was controlled by the precursor bottle temperature and the pneumatic valve open time. The dosing time for Ti(O<sup>i</sup>Pr)<sub>4</sub> was set to 50 ms to keep the pressure size rise small to avoid unwanted CVD reactions. The dosing times for

AcOH and HCO<sub>2</sub>H were set to 90 ms (AcOH) and 60 ms (HCO<sub>2</sub>H) to have similar-size second precursor pressure. During single-precursor TiO<sub>2</sub> CVD, Ti(O<sup>i</sup>Pr)<sub>4</sub> was dosed with the above-mentioned dosing conditions. For ALD and CVD, multiple short precursor pulses are commonly used instead of single long pulses to avoid pumping high pressures with the turbomolecular pump. The repeated short pulses also allow time for residues to desorb from the reaction surface in ALD reactions and in unimolecular pulsed CVD reactions. Between each Ti(O<sup>i</sup>Pr)<sub>4</sub> pulse, a 5 s purge was used to remove residual precursors and reaction byproducts. For the ALD process to deposit appreciable TiO<sub>2</sub>, 20 pulses of Ti(O<sup>i</sup>Pr)<sub>4</sub> were required per 1 pulse of AcOH or HCO<sub>2</sub>H (see Supporting Information, Figure S1 for additional information). The purge duration between Ti(O<sup>i</sup>Pr)<sub>4</sub> and the second precursor (AcOH or HCO<sub>2</sub>H) was 60 s.

After deposition, each sample was transferred to an X-ray photoelectron spectroscopy (XPS) system for *in vacuo* XPS analysis. The XPS measurement used a monochromatic Al K $\alpha$  source (1486.7 eV) with an XM 1000 MkII/SPHERA X-ray source from Omicron Nanotechnology. The spectra were measured with constant analyzer energy with a pass energy of 50 eV and a step width of 0.1 eV. The angle between the analyzer normal and the sample surface was 30°. The peak shape analysis was performed with the CASA XPS v.2.3 program using Shirley background subtraction. After deposition and XPS, atomic force microscopy (AFM) and grazing incidence X-ray diffraction (GIXRD) were performed *ex situ*.

The TiO<sub>2</sub> film thickness was derived using the inelastic mean free path (IMFP) and attenuation length of an electron from the Si substrate as given below.<sup>6</sup>

$$t = \lambda \sin \theta \ln \left( \frac{I_0}{I} \right)$$

$$\lambda = \frac{143}{E^2} + 0.054\sqrt{E}$$

$t$  is the film thickness on the substrate,  $\lambda$  is the IMFP of the electrons from the Si substrate,  $\theta$  is the angle of an emitted electron from the surface,  $I$  is the intensity of the substrate signal (after deposition),  $I_0$  is the intensity of the unattenuated substrate signal (before deposition), and  $E$  is the kinetic energy of the electrons. The thickness derived from the equation mentioned above showed similar thickness (a few angstrom difference) compared to the thickness from ellipsometry. However, if the deposition on the Si substrate exceeds  $\sim 4$  nm, the Si substrate peak is fully attenuated ( $I = 0$ ), and the above equation is not applicable. Therefore, when the Si substrate peak was fully attenuated, the thickness was measured with *ex situ* ellipsometry. When the deposition was below  $\sim 1$  nm, it is possible that the deposition is not a continuous film and only TiO<sub>2</sub> nuclei are present. However, even for sub 1 nm films, the XPS attenuation equation was employed to determine a nominal film thickness.

### 3. RESULTS AND DISCUSSION

**3.1. TiO<sub>2</sub> ALD with Ti(O<sup>i</sup>Pr)<sub>4</sub> and AcOH.** Consistent with the previous research on water-free ALD by Ramos *et al.*,<sup>21</sup> the selective ALD of TiO<sub>2</sub> using Ti(O<sup>i</sup>Pr)<sub>4</sub> and AcOH was tested on Si, SiO<sub>2</sub>, and SiCOH. Each ALD cycle contained 20 pulses of Ti(O<sup>i</sup>Pr)<sub>4</sub> and 1 pulse of AcOH, as mentioned in detail in the Experimental Section. Figure 2 shows the chemical composition as determined by XPS of three samples and AFM images of the surfaces after the TiO<sub>2</sub> deposition (XPS spectra are shown for each of the element-specific regions in Supporting Information, Figure S2). The XPS results show that after the first 40 ALD cycles, 10 and 8% of Ti were detected on Si and SiO<sub>2</sub> surfaces, respectively, while no significant Ti was detected from the SiCOH surface. After additional 100 ALD cycles, 1.7 and 1.3 nm of TiO<sub>2</sub> were deposited on Si and SiO<sub>2</sub>, respectively. The thicknesses of TiO<sub>2</sub> films were calculated based on the attenuation of Si

substrate signals.<sup>6</sup> After these 100 additional cycles, nucleation was observed on SiCOH with 3% of Ti, which is still less than a monolayer of TiO<sub>2</sub> ( $\sim 0.4$  nm).<sup>29</sup> After an additional 100 ALD cycles (240 ALD cycles total), the thickness of TiO<sub>2</sub> was 2.8 nm on Si and 2.3 nm on SiO<sub>2</sub>. Since XPS is a surface-sensitive measurement, as deposition increases beyond  $\sim 2$  nm with the same deposition process, TiO<sub>2</sub> films with similar O, C, and Ti ratios are deposited and show nearly constant O, C, and Ti XPS fractions. The TiO<sub>2</sub> thicknesses on Si and SiO<sub>2</sub> were similar in the 2–3 nm range as AcOH reacted on both surfaces and induced similar reactivities on both surfaces; it is likely that both surfaces had sufficient -OAc groups to nucleate reaction with the precursors. On SiCOH, 0.4 nm of the TiO<sub>2</sub> film had accumulated; nucleation was slower on SiCOH than that on Si and SiO<sub>2</sub>. This is consistent with Si-OC<sub>x</sub>H<sub>y</sub> or Si-C<sub>x</sub>H<sub>y</sub> groups on the SiCOH surface preventing the reaction with precursors, thus inducing inherently selective deposition.

After deposition, *ex situ* AFM was performed to quantify the surface morphology (Figure 2). The TiO<sub>2</sub> film on Si, which had a total thickness of 2.8 nm, showed 2 Å rms roughness. The TiO<sub>2</sub> on SiO<sub>2</sub>, which had a total thickness of 2.3 nm, showed 3 Å rms roughness. Both films were smooth with low rms roughness and no significant particles. The TiO<sub>2</sub> on SiCOH, which had a total thickness of 0.4 nm, showed 8 Å rms roughness. Several particles with  $\sim 6$  nm height were detected on the SiCOH surface. However, these particles with high rms roughness were also observed on a degreased SiCOH surface with no deposition (7 Å rms roughness, see Supporting Information, Figure S3). Since the deposition tends to occur earlier on heterogeneous surfaces such as step edges or defect sites, which are plentiful on particles and high-roughness surfaces,<sup>10</sup> it might be possible to obtain higher selectivity if SiCOH with lower surface roughness was employed.

To verify the TiO<sub>2</sub> ALD reaction between Ti(O<sup>i</sup>Pr)<sub>4</sub> and AcOH, the reaction mechanism was studied using XPS. Figure 3 shows the carbon 1s XPS spectra of a TiO<sub>2</sub> film grown on Si after sequential doses of each precursor at 250 °C. Each curve was the sum of 10 XPS sweeps to reduce the background noise.

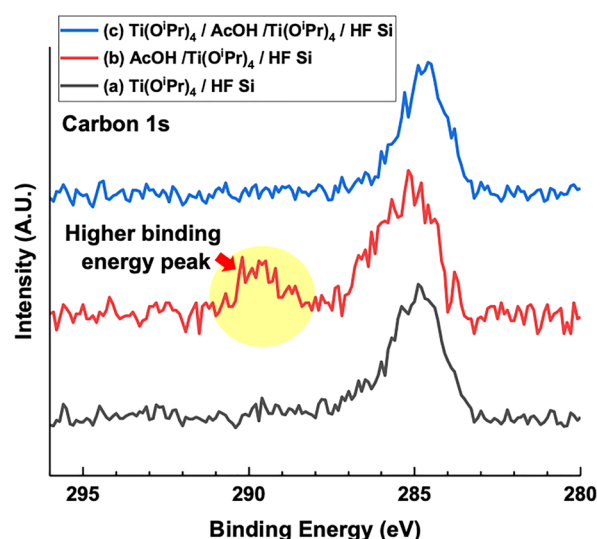


**Figure 3.** Carbon 1s XPS spectra of a TiO<sub>2</sub> film grown on Si after Ti(O<sup>i</sup>Pr)<sub>4</sub> and AcOH half cycles at 250 °C. (a) Carbon 1s peak after a total 2000 pulses of Ti(O<sup>i</sup>Pr)<sub>4</sub> at 250 °C. (b) Carbon 1s peak after dosing AcOH. (c) Carbon 1s peak after the additional dosing of Ti(O<sup>i</sup>Pr)<sub>4</sub>.

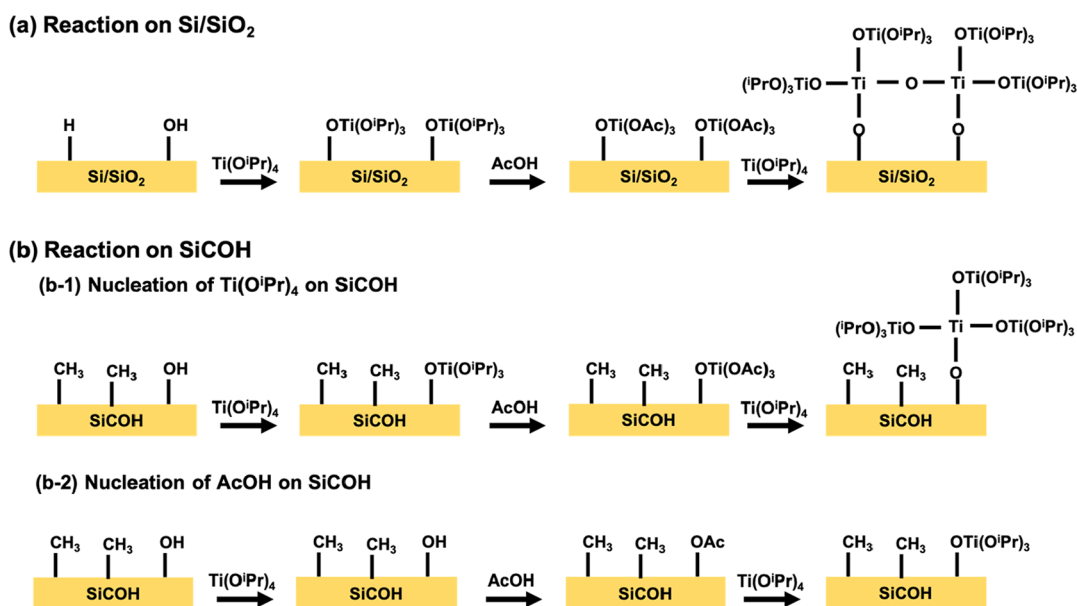


**Figure 4.** Reaction schematic showing the ALD reaction between  $\text{Ti}(\text{O}^i\text{Pr})_4$  and AcOH on Si/SiO<sub>2</sub> and SiCOH. (a) On Si/SiO<sub>2</sub>, as each precursor is sequentially dosed, ligand exchange between  $-\text{O}^i\text{Pr}$  and  $-\text{OAc}$  bonds occurs and forms  $\text{TiO}_2$ . (b) SiCOH surface is predominantly terminated with alkyl groups. Therefore,  $\text{Ti}(\text{O}^i\text{Pr})_4$  (b-1) and AcOH (b-2) can react only on a small number of  $-\text{OH}$  defects, but these induce the loss of selectivity.

After 2000 pulses of  $\text{Ti}(\text{O}^i\text{Pr})_4$ , nucleation occurred on the Si surface, and carbon had a binding energy of 284–287 eV (Figure 3a) which corresponds to the  $\text{Ti}-\text{O}^i\text{Pr}$  bonds.<sup>30</sup> When AcOH was sequentially dosed, a peak at higher binding energy appeared (Figure 3b). This higher-binding-energy peak is consistent with surface  $-\text{OAc}$  bonds from  $-\text{OAc}$  groups remaining on the surface after AcOH doses. However, the subsequently dosed  $\text{Ti}(\text{O}^i\text{Pr})_4$  had ligand exchange with the surface  $-\text{OAc}$  bond and bonded on the surface (Figure 3c). Due to this ligand exchange, the  $-\text{OAc}$  bonds were removed, and  $-\text{O}^i\text{Pr}$  bonds were on the surface. Consequently, the Figure 3c spectrum did not have a high-binding-energy peak but showed similar binding energy to the Figure 3a spectrum. The XPS spectra show that the precursors in each half cycle had ALD reactions with ligand exchange. In addition, an experiment on  $\text{TiO}_2$  growth with multiple pulses of  $\text{Ti}(\text{O}^i\text{Pr})_4$  and AcOH showed that the  $\text{TiO}_2$  growth is mainly due to the ALD reaction between  $\text{Ti}(\text{O}^i\text{Pr})_4$  and AcOH with a minor thermal CVD component from  $\text{Ti}(\text{O}^i\text{Pr})_4$ . (The detailed experimental results and explanation are shown in Supporting Information, Figure S4.)

The carbon XPS spectra study confirmed the ALD mechanism, as shown in Figure 4. On Si/SiO<sub>2</sub>,  $\text{Ti}(\text{O}^i\text{Pr})_4$  starts to nucleate on the surface and forms  $-\text{O}-\text{Ti}-\text{O}^i\text{Pr}$  bonds. As AcOH is subsequently dosed, ligand exchange between  $-\text{O}^i\text{Pr}$  and  $-\text{OAc}$  occurs and forms surface-bound  $-\text{O}-\text{Ti}-\text{OAc}$ . The higher-binding-energy carbon 1s peak from Figure 3b is from the  $-\text{OAc}$  group. This  $-\text{OAc}$  group is reactive toward subsequent  $\text{Ti}(\text{O}^i\text{Pr})_4$  and induces subsequent ligand exchange, and thus, the higher-binding-energy carbon peak disappeared (Figure 3c). With this ligand exchange,  $\text{TiO}_2$  is formed on the Si surface. In contrast to Si and SiO<sub>2</sub>, the SiCOH surface is predominantly terminated with alkyl groups. These alkyl groups are less reactive to precursors compared to the  $-\text{H}$  termination on Si and  $-\text{OH}$  termination on SiO<sub>2</sub>. On SiCOH, the precursors can only react on sparse defect  $-\text{OH}$  sites and thus nucleate slowly. However, since SiCOH is SiO<sub>2</sub>

passivated with the  $\text{Si}-\text{OC}_x\text{H}_y$  or  $\text{Si}-\text{C}_x\text{H}_y$  group,<sup>24–26</sup> the exact density of  $-\text{OH}$  defect sites among major  $\text{Si}-\text{OC}_x\text{H}_y$  or  $\text{Si}-\text{C}_x\text{H}_y$  groups on SiCOH cannot be quantified with a standard XPS spectrometer such as the one employed in the present study. This nucleation on defects eventually induces the loss of selectivity as dosing continues.

**3.2.  $\text{TiO}_2$  ALD with  $\text{Ti}(\text{O}^i\text{Pr})_4$  and  $\text{HCO}_2\text{H}$ .** From the above experiment, it was found that  $\text{TiO}_2$  ALD can occur with  $\text{Ti}(\text{O}^i\text{Pr})_4$  and AcOH through the ligand exchange. Based on this finding, it was hypothesized that other carboxylic acids may also have a similar reaction with  $\text{Ti}(\text{O}^i\text{Pr})_4$ . Formic acid ( $\text{HCO}_2\text{H}$ ) has a  $\text{pK}_a$  of 3.7, while acetic acid has a  $\text{pK}_a$  of 4.7. This stronger acidity means formic acid can be a 10× stronger proton donor than acetic acid. As formic acid may have 10× higher reactivity in ALD reactions,<sup>26</sup> it can induce a larger portion of the subsequently dosed  $\text{Ti}(\text{O}^i\text{Pr})_4$  to react with the surface formate bonds than the acetate bonds from AcOH. The ALD reaction with  $\text{Ti}(\text{O}^i\text{Pr})_4$  and formic acid was tested to verify whether it shows faster growth and greater selectivity.

Figure 5 shows the XPS chemical composition (XPS spectra for each element-specific binding region are shown in Supporting Information, Figure S5) and AFM images of each substrate after 20 ALD cycles of  $\text{Ti}(\text{O}^i\text{Pr})_4$  and  $\text{HCO}_2\text{H}$ . After 20 ALD cycles, 2.4 and 2.2 nm of  $\text{TiO}_2$  were deposited on Si and SiO<sub>2</sub>, respectively. Conversely, only ~0.3 nm  $\text{TiO}_2$  was detected on SiCOH. As expected,  $\text{HCO}_2\text{H}$  was more reactive than AcOH; 20 ALD cycles with  $\text{HCO}_2\text{H}$  had a similar thickness of  $\text{TiO}_2$  deposition to 240 ALD cycles with AcOH, indicating that  $\text{HCO}_2\text{H}$  has around 10× higher reactivity than AcOH. However, even though different carboxylic acids were used, both experiments showed a similar selectivity of around 2–3 nm of  $\text{TiO}_2$  deposition on Si and SiO<sub>2</sub> and around a monolayer deposition (~0.4 nm)<sup>29</sup> on SiCOH (sub 1 nm deposition on SiCOH can be  $\text{TiO}_2$  nuclei; however, even for the films, the XPS attenuation equation was employed to determine a nominal film thickness). This observation shows that the carboxylic acid second precursors have only a minor

**TiO<sub>2</sub> ALD cycle:**  
**20xTi(O<sup>i</sup>Pr)<sub>4</sub> + 1x HCO<sub>2</sub>H / cycle with continuous N<sub>2</sub> purge @ 250 °C**

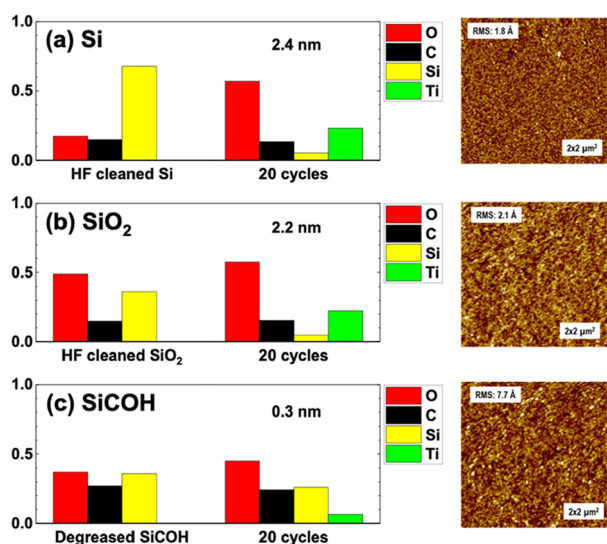


**Figure 5.** XPS chemical composition (left) and AFM image (right) of the TiO<sub>2</sub> film after 20 ALD cycles of Ti(O<sup>i</sup>Pr)<sub>4</sub> and HCO<sub>2</sub>H at 250 °C. (a) HF-cleaned Si: 2.4 nm of TiO<sub>2</sub> was deposited and the film was smooth with an rms roughness of 1.8 Å. (b) HF-cleaned SiO<sub>2</sub>: 2.2 nm of TiO<sub>2</sub> was deposited and the film was smooth with an rms roughness of 2.1 Å. (c) Degreased SiCOH: Around 0.3 nm of TiO<sub>2</sub> was deposited and the surface rms roughness was 7.7 Å, which is similar to that of the bare SiCOH surface.

effect on selectivity. Therefore, the loss of selectivity of TiO<sub>2</sub> ALD could be mainly due to the reaction of Ti(O<sup>i</sup>Pr)<sub>4</sub> with the SiCOH surface; as a metal alkoxide precursor, Ti(O<sup>i</sup>Pr)<sub>4</sub> contains oxygen atoms and can therefore react with defect sites to nucleate on SiCOH. This ultimately causes a loss of selectivity.

Figure 5 shows the AFM images of the TiO<sub>2</sub> films on Si, SiO<sub>2</sub>, and SiCOH. The rms roughnesses of the TiO<sub>2</sub> film on Si and SiO<sub>2</sub> were 1.8 and 2.1 Å, respectively. The rms roughness on SiCOH was 7.7 Å similar to that of a degreased SiCOH surface (Supporting Information, Figure S3). These results show that TiO<sub>2</sub> ALD using HCO<sub>2</sub>H has a 10× greater growth rate but produces films with similar selectivity and roughness compared to ALD with AcOH.

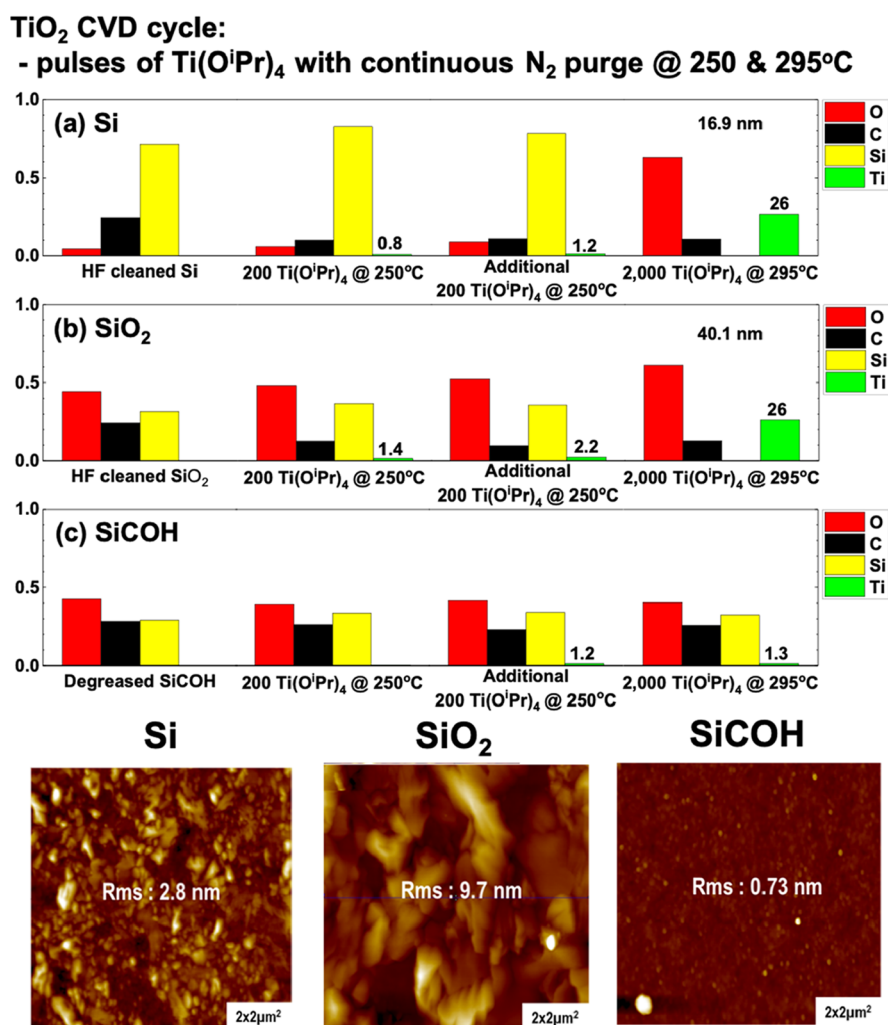
**3.3. TiO<sub>2</sub> Single-Precursor Thermal CVD with Ti(O<sup>i</sup>Pr)<sub>4</sub>.** It was previously reported that Ti(O<sup>i</sup>Pr)<sub>4</sub> thermally decomposes and undergoes unimolecular CVD at 250 °C.<sup>1</sup> Therefore, single-precursor pulsed CVD with Ti(O<sup>i</sup>Pr)<sub>4</sub> was performed to determine the inherent selectivity.

Figure 6 shows the XPS chemical composition of TiO<sub>2</sub> films on Si, SiO<sub>2</sub>, and SiCOH deposited by the pulsed CVD process. (XPS spectra of each element-specific binding region are shown in Supporting Information, Figure S6.) At first, CVD was tested at 250 °C: after 400 pulses of Ti(O<sup>i</sup>Pr)<sub>4</sub>, Ti compositions of 1.2, 2.2, and 1.2% were observed on Si, SiO<sub>2</sub>, and SiCOH, respectively. This indicates that only TiO<sub>2</sub> nuclei were formed on each substrate. Compared to the 2–3 nm of TiO<sub>2</sub> deposited on Si and SiO<sub>2</sub> during ALD with HCO<sub>2</sub>H with the same number of Ti(O<sup>i</sup>Pr)<sub>4</sub> pulses, the growth rate by unimolecular CVD at 250 °C was minuscule. This indicates that the precursor does not undergo significant thermal decomposition on a 250 °C substrate.

Since CVD at 250 °C left an almost clean SiCOH surface, an additional inherent selectivity test with higher-temperature CVD was made on the same SiCOH sample. The sample temperature was increased to 295 °C to promote thermal decomposition in the pulsed CVD reaction. After 2000 pulses of Ti(O<sup>i</sup>Pr)<sub>4</sub>, Si peaks (Si 2p) were fully attenuated on Si and SiO<sub>2</sub> substrates, which means that more than ~4 nm (without knowing the exact film thickness on Si and SiO<sub>2</sub> from the XPS result) of TiO<sub>2</sub> was deposited on both substrates. From ellipsometry, the precise thicknesses of TiO<sub>2</sub> on Si and SiO<sub>2</sub> were 16.9 and 40.1 nm, respectively. Compared to previous ALD results, which showed films of equivalent thicknesses, significantly more TiO<sub>2</sub> deposition occurred on SiO<sub>2</sub> than on Si, which showed potential in selective TiO<sub>2</sub> deposition on SiO<sub>2</sub> in preference to Si. This shorter induction period on SiO<sub>2</sub> is attributed to the higher reactivity of the hydroxyl-terminated surface on SiO<sub>2</sub> than the hydrogen-terminated surface on Si. For the pulsed unimolecular thermal CVD process, after 2000 Ti(O<sup>i</sup>Pr)<sub>4</sub> pulses at 295 °C, a composition of only 1.3% of Ti was detected on SiCOH (most of this was deposited during the prior 250 °C CVD test), showing that the CVD reaction at 295 °C has high selectivity.

These ALD and CVD experiments at two different sample temperatures show that temperature can affect the selectivity. From ALD with two different carboxylic acids, it was proven that the carboxylic acids have a minor effect on selectivity. The loss of selectivity could be due to the nucleation of Ti(O<sup>i</sup>Pr)<sub>4</sub> on the SiCOH surface. Therefore, the higher selectivity at 295 °C unimolecular CVD may be due to the higher sample temperature promoting the desorption of Ti(O<sup>i</sup>Pr)<sub>4</sub> on the SiCOH surface before it nucleates.

*Ex situ* AFM was performed to check the film morphology. Figure 6 shows the atomic force micrograph of each sample. Si and SiO<sub>2</sub>, which had thick TiO<sub>2</sub> depositions of 16.9 and 40.1 nm, respectively, showed 2.8 and 9.7 nm rms roughnesses, respectively (AFM scans with line traces are shown in Supporting Information, Figure S7). Sparse TiO<sub>2</sub> nuclei are observed on SiCOH, and the rms roughness was 0.73 nm, which was close to that of a degreased SiCOH. The increase in rms roughness on the Si and SiO<sub>2</sub> surface is due to the crystallization of the TiO<sub>2</sub> film. Figure 7 shows the GIXRD results for the films on Si and SiO<sub>2</sub> from Figure 6. The 16.9 nm thick TiO<sub>2</sub> film on Si showed a small anatase (100) peak (inset of Figure 7a). The crystallization became more significant for the TiO<sub>2</sub> film on SiO<sub>2</sub> (40.1 nm) since it was a thicker film than the film on Si (Figure 7b).<sup>31</sup> GIXRD for SiO<sub>2</sub> showed anatase (100), (200), and (204) peaks. In addition, the intensity for the (100) peak from the SiO<sub>2</sub> substrate was higher than that from the Si substrate because the film on SiO<sub>2</sub> was thicker. The peaks observed at 51 and 55° are from the Si(113) peak and the XRD sample stage, respectively. In addition, the 2 nm TiO<sub>2</sub> film from the same CVD process showed a smooth film with 0.4 nm rms roughness (Supporting Information, Figure S8). These results show that the thicker TiO<sub>2</sub> film was more crystalline, which is consistent with the increased roughness observed by AFM (Figure 6). This effect is well-known in the literature; the crystallization temperature of an oxide film decreases as the film thickness increases.<sup>31</sup> This crystallization issue can be problematic for the potential application of selective TiO<sub>2</sub> deposition in nanoscale patterning and could be avoided by periodically inserting a second oxide layer into the film to form a nanolaminate structure.<sup>27,28</sup>



**Figure 6.** XPS chemical composition (above) and AFM (below) of (a) HF-cleaned Si, (b) HF-cleaned SiO<sub>2</sub>, and (c) degreased SiCOH after doses of Ti(O<sup>i</sup>Pr)<sub>4</sub> at 250 and 295 °C. After 400 pulses of Ti(O<sup>i</sup>Pr)<sub>4</sub> at 250 °C, there is only a small amount of Ti on all three samples. After 2000 pulses of Ti(O<sup>i</sup>Pr)<sub>4</sub> at 295 °C, there is 16.9 nm TiO<sub>2</sub> deposited on Si and 40.1 nm TiO<sub>2</sub> on SiO<sub>2</sub>, while there is only 1.3% Ti on SiCOH. AFM images show that the TiO<sub>2</sub> films on Si, SiO<sub>2</sub>, and SiCOH have rms roughnesses of 2.8, 9.7, and 0.7 nm, respectively.

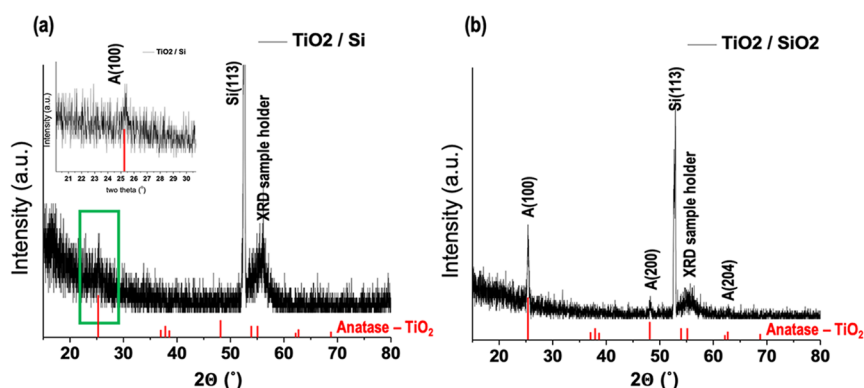


**Figure 7.** GIXRD curves for (a) Si and (b) SiO<sub>2</sub> after TiO<sub>2</sub> CVD at 295 °C (samples from Figure 6). (a) 16.9 nm TiO<sub>2</sub> on Si showed a small TiO<sub>2</sub> anatase (100) peak, as shown in the inset of (a). (b) 40.1 nm TiO<sub>2</sub> on SiO<sub>2</sub> showed TiO<sub>2</sub> anatase (100), (200), and (204) peaks. The peaks observed at 51 and 55° from both samples are from the Si(113) peak from the substrates and the XRD sample holder, respectively.

**3.4. Nanoscale Selectivity of TiO<sub>2</sub> CVD.** Selectivity tests for the TiO<sub>2</sub> ALD and pulsed unimolecular CVD process showed that the pulsed unimolecular CVD process with Ti(O<sup>i</sup>Pr)<sub>4</sub> at 295 °C had the highest selectivity. Therefore, TiO<sub>2</sub> CVD at 295 °C was tested on Cu/SiCOH nanoscale

patterned samples to determine the selectivity of deposition on the nanometer scale. Nanoscale selective deposition for the ALD process was not tested as ALD had a low selective deposition (~2 nm), which is difficult to detect with transmission electron microscopy (TEM). As mentioned in

the Experimental Section, since the SiCOH region of the patterned sample was damaged and likely contained significantly more defect sites than a blanket SiCOH wafer surface, additional passivation (proprietary passivation process from Applied Materials) was performed before loading the sample into the deposition chamber. The Cu region of the patterned sample also went through the passivation process; however, the passivant on the Cu surface desorbed during a subsequent UHV anneal (350 °C for 30 min, as determined by XPS of the carbon from Supporting Information, Figure S9) before the CVD process. In this way, only the SiCOH region of the patterned sample was selectively passivated against TiO<sub>2</sub> deposition. When loading the above patterned sample, a SiCOH blanket sample with the same passivation was also loaded to serve as a reference.

Supporting Information, Figure S9 shows the XPS chemical composition of a passivated SiCOH and a passivated Cu/SiCOH patterned sample before and after doses of Ti(O<sup>i</sup>Pr)<sub>4</sub> at 295 °C. XPS spectra of each element are shown in Supporting Information, Figure S10. After 300 pulses of Ti(O<sup>i</sup>Pr)<sub>4</sub>, the blanket SiCOH substrate still remained deposition-free, with no Ti peaks observed by XPS. For the Cu/SiCOH patterned sample, after 300 Ti(O<sup>i</sup>Pr)<sub>4</sub> pulses, the Cu 2p peak disappeared and a Ti 2p peak corresponding to 12 at. % Ti appeared. This means that a TiO<sub>2</sub> film was deposited on the exposed Cu surface of the patterned substrate. The Si peak maintained similar XPS abundance before and after deposition on the patterned sample, suggesting that there was no TiO<sub>2</sub> deposition on the SiCOH region of the patterned sample, as also observed on the blanket SiCOH substrate.

The selectivity of the process was documented using cross-sectional TEM, as shown in Figure 8. The widths of Cu and

that the TiO<sub>2</sub> film on Cu showed a very rough surface which is likely due to crystallization, but as previously noted, using nanolaminates can produce smooth films.<sup>27,28</sup> Therefore, based on the TEM study of TiO<sub>2</sub> unimolecular CVD at 295 °C, it is proven that the process can selectively deposit TiO<sub>2</sub> films in nanoscale regions.

#### 4. CONCLUSIONS

Inherent selective TiO<sub>2</sub> deposition on Si and SiO<sub>2</sub> in preference to SiCOH (a porous low-*k* dielectric) with ALD and CVD was investigated. Water-free deposition was tested both to protect SiCOH and to enhance selectivity. At 250 °C sample temperature, selective water-free ALD of TiO<sub>2</sub> using Ti(O<sup>i</sup>Pr)<sub>4</sub> and AcOH was accomplished. This ALD process achieved around 1.5 nm of selective TiO<sub>2</sub> deposition on Si and SiO<sub>2</sub>, while less than a monolayer (3% Ti from XPS measurement) was deposited on SiCOH. AFM showed that the TiO<sub>2</sub> films on Si and SiO<sub>2</sub> were smooth with 2 and 3 Å rms roughness, respectively. An XPS study showed that TiO<sub>2</sub> was deposited through the ligand exchange reaction between the isopropoxide ligand (–O<sup>i</sup>Pr) of Ti(O<sup>i</sup>Pr)<sub>4</sub> and acetate ligand (–OAc) of AcOH. For ALD with Ti(O<sup>i</sup>Pr)<sub>4</sub> and HCO<sub>2</sub>H at 250 °C sample temperature, the growth rate increased by a factor of ~10× compared to ALD with AcOH while maintaining similar selectivity. This is consistent with chemical intuition that HCO<sub>2</sub>H acts as a stronger proton donor than AcOH. The TiO<sub>2</sub> films deposited by ALD using HCO<sub>2</sub>H were smooth with an rms roughness of around 2 Å on Si and SiO<sub>2</sub>. The selectivity of both ALD showed that the loss of selectivity is mainly due to the nucleation of Ti(O<sup>i</sup>Pr)<sub>4</sub> on the SiCOH surface and not related to carboxylic acid second precursors such as AcOH and HCO<sub>2</sub>H. Single-precursor CVD by the thermal decomposition of Ti(O<sup>i</sup>Pr)<sub>4</sub> was studied; at 295 °C, highly selective deposition of TiO<sub>2</sub> was achieved with 16.9 nm on Si and 40.1 nm on SiO<sub>2</sub>. However, these thick TiO<sub>2</sub> films were prone to crystallization and had an rms roughness of more than 1 nm. The nanolaminate structure can solve this crystallization issue;<sup>27,28</sup> thus, further study on inherent selective nanolaminate oxide deposition is required. In addition, the TiO<sub>2</sub> film from both ALD and CVD showed 10–20% surface carbon; if there is high carbon in the entire depth of the film, the carbon may degrade its electrical performance. As observed by TEM, single-precursor CVD at 295 °C on patterned substrates exhibits selective deposition on Cu with minimal deposition on SiCOH, which demonstrates the utility of the unimolecular CVD process in nanoscale patterning applications. Further optimization with a nanolaminate CVD process will form a high-selective smooth film and further enable its applications in the patterning process for nanometer-scale MOSFET fabrication.

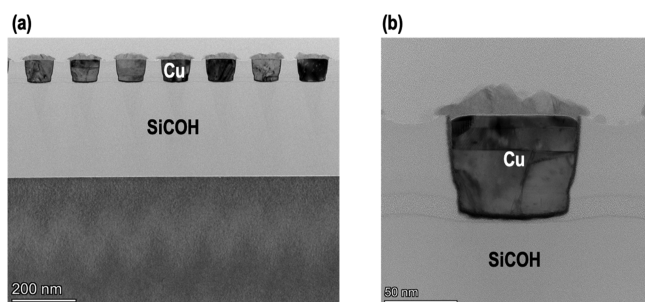


**Figure 8.** TEM of selective TiO<sub>2</sub> deposition on a Cu/SiCOH patterned sample: (a) TEM image after TiO<sub>2</sub> unimolecular CVD with Ti(O<sup>i</sup>Pr)<sub>4</sub> at 295 °C (300 pulses total) on a Cu/SiCOH patterned sample and (b) magnified view of a Cu inlay. As can be seen from TEM images, TiO<sub>2</sub> was selectively deposited on the Cu surface only. The film thickness was around 20 nm and the film roughened, likely due to crystallization as in previous experiments.

SiCOH regions on the sample surface were ~90 and ~50 nm, respectively. The low-magnification micrograph (Figure 8a) shows that TiO<sub>2</sub> was only deposited on the Cu regions of the patterned sample. No significant TiO<sub>2</sub> deposition was observed on any SiCOH surface. The magnified view of the patterned inlay (Figure 8b) shows around 20 nm of TiO<sub>2</sub> deposited on the Cu with slight protrusion onto the neighboring SiCOH due to the lateral growth of the TiO<sub>2</sub> material. This lateral growth of TiO<sub>2</sub> could be due to the physisorbed Ti(O<sup>i</sup>Pr)<sub>4</sub> precursor on the SiCOH surface, which diffused and reacted on the sidewall of the TiO<sub>2</sub> film on Cu; however, further study is required. It is again seen from the TEM image on Figure 8

#### ■ ASSOCIATED CONTENT

##### Supporting Information

The Supporting Information is available free of charge at <https://pubs.acs.org/doi/10.1021/acsnm.1c03311>.

XPS chemical composition of Si, SiO<sub>2</sub>, and SiCOH before/after 20 cycles of TiO<sub>2</sub> ALD with Ti(O<sup>i</sup>Pr)<sub>4</sub> and AcOH (1:1 pulse ratio); XPS spectra of each element on each sample during each process of TiO<sub>2</sub> ALD with AcOH; AFM image of degreased SiCOH without any oxide deposition; XPS chemical composition and table for the TiO<sub>2</sub> deposition test with multiple-pulse half

cycles of  $\text{Ti}(\text{O}^i\text{Pr})_4$  and  $\text{AcOH}$ ; XPS spectra of each element on each sample during each process of  $\text{TiO}_2$  ALD with  $\text{HCO}_2\text{H}$ ; XPS spectra of each element on each sample during each process of  $\text{TiO}_2$  CVD; AFM images and line traces of the  $\text{TiO}_2$  film on the Si and  $\text{SiO}_2$  substrate after  $\text{TiO}_2$  CVD; XPS chemical composition and AFM image for the  $\sim 2$  nm  $\text{TiO}_2$  film deposited by  $\text{Ti}(\text{O}^i\text{Pr})_4$  CVD at  $300^\circ\text{C}$ ; XPS chemical composition of passivated  $\text{SiCOH}$  and passivated  $\text{Cu}/\text{SiCOH}$  nanoscale patterned sample before and after  $\text{TiO}_2$  CVD; and XPS spectra of each element on each sample during each process of the  $\text{TiO}_2$  CVD nanoscale selectivity test (PDF)

## AUTHOR INFORMATION

### Corresponding Author

Andrew C. Kummel – Department of Chemistry & Biochemistry, University of California, San Diego, La Jolla, California 92093, United States; [orcid.org/0000-0001-8301-9855](https://orcid.org/0000-0001-8301-9855); Email: [akummel@ucsd.edu](mailto:akummel@ucsd.edu)

### Authors

Yunil Cho – Electrical and Computer Engineering Program, University of California, San Diego, La Jolla, California 92093, United States; [orcid.org/0000-0002-2680-2015](https://orcid.org/0000-0002-2680-2015)

Christopher F. Ahles – Materials Science and Engineering Program, University of California, San Diego, La Jolla, California 92093, United States

Jong Youn Choi – Materials Science and Engineering Program, University of California, San Diego, La Jolla, California 92093, United States; [orcid.org/0000-0001-7415-3091](https://orcid.org/0000-0001-7415-3091)

James Huang – Materials Science and Engineering Program, University of California, San Diego, La Jolla, California 92093, United States

Antony Jan – Applied Materials, Sunnyvale, California 95054, United States

Keith Wong – Applied Materials, Sunnyvale, California 95054, United States

Srinivas Nemani – Applied Materials, Sunnyvale, California 95054, United States

Ellie Yieh – Applied Materials, Sunnyvale, California 95054, United States

Complete contact information is available at: <https://pubs.acs.org/10.1021/acsnm.1c03311>

### Notes

The authors declare no competing financial interest.

## ACKNOWLEDGMENTS

Funding support from Applied Materials is gratefully appreciated. The electrical measurements were facilitated by the San Diego Nanotechnology Infrastructure (SDNI) which is supported by the National Science Foundation (NSF) to Nano3 (grant ECCS-1542148).

## REFERENCES

(1) Atanasov, S. E.; Kalanyan, B.; Parsons, G. N. Inherent substrate-dependent growth initiation and selective-area atomic layer deposition of  $\text{TiO}_2$  using “water-free” metal-halide/metal alkoxide reactants. *J. Vac. Sci. Technol., A* **2016**, *34*, 01A148.

(2) Li, H.; Farmer, D. B.; Gordon, R. G.; Lin, Y.; Vlassak, J. Vapor Deposition of Ruthenium from an Amidinate Precursor. *J. Electrochem. Soc.* **2007**, *154*, D642–D647.

(3) [www.beneq.com/en/technology](https://www.beneq.com/en/technology) (last access Nov 29, 2021).

(4) Lee, H.-B.; Bent, S. F. A Selective Toolbox for Nanofabrication. *Chem. Mater.* **2020**, *32*, 3323–3324.

(5) Mackus, A. J. M.; Bol, A. A.; Kessels, W. M. M. The use of atomic layer deposition in advanced nanopatterning. *Nanoscale* **2014**, *6*, 10941–10960.

(6) Choi, J. Y.; Ahles, C. F.; Cho, Y.; Anurag, A.; Wong, K. T.; Nemani, S. D.; Yieh, E.; Kummel, A. C. Selective pulsed chemical vapor deposition of water-free  $\text{HfO}_x$  on Si in preference to  $\text{SiCOH}$  and passivated  $\text{SiO}_2$ . *Appl. Surf. Sci.* **2020**, *512*, 145733.

(7) Yang, M.; Aarnink, A. A. I.; Schmitz, J.; Kovalgin, A. Y. Inherently area-selective hot-wire assisted atomic layer deposition of tungsten films. *Thin Solid Films* **2018**, *649*, 17–23.

(8) Choi, J. Y.; Ahles, C. F.; Hung, R.; Kim, N.; Kummel, A. C. Selective atomic layer deposition of  $\text{MoSi}_x$  on Si (001) in preference to silicon nitride and silicon oxide. *Appl. Surf. Sci.* **2018**, *462*, 1008–1016.

(9) Lemaire, P. C.; King, M.; Parsons, G. N. Understanding inherent substrate selectivity during atomic layer deposition: Effect of surface preparation, hydroxyl density, and metal oxide composition on nucleation mechanisms during tungsten ALD. *J. Chem. Phys.* **2017**, *146*, 052811.

(10) Cao, K.; Cai, J.; Chen, R. Inherently Selective Atomic Layer Deposition and Applications. *Chem. Mater.* **2020**, *32*, 2195–2207.

(11) Bobb-Semple, D.; Nardi, K. L.; Draeger, N.; Hausmann, D. M.; Bent, S. F. Area-Selective Atomic Layer Deposition Assisted by Self-Assembled Monolayers: A Comparison of Cu, Co, W, and Ru. *Chem. Mater.* **2019**, *31*, 1635–1645.

(12) Hashemi, F. S. M.; Bent, S. F. Sequential Regeneration of Self-Assembled Monolayers for Highly Selective Atomic Layer Deposition. *Adv. Mater. Interfaces* **2016**, *3*, 1600464.

(13) Hashemi, F. S. M.; Prasittichai, C.; Bent, S. F. A new resist for area selective atomic and molecular layer deposition on metal-dielectric patterns. *J. Phys. Chem. C* **2014**, *118*, 10957.

(14) Prasittichai, C.; Pickrahn, K. L.; Hashemi, F. S. M.; Bergsman, D. S.; Bent, S. F. Improving Area-Selective Molecular Layer Deposition by Selective SAM Removal. *ACS Appl. Mater. Interfaces* **2014**, *6*, 17831–17836.

(15) Hashemi, F. S. M.; Birchansky, B. R.; Bent, S. F. Selective Deposition of Dielectrics: Limits and Advantages of Alkanethiol Blocking Agents on Metal-Dielectric Patterns. *ACS Appl. Mater. Interfaces* **2016**, *8*, 33264–33272.

(16) Mamel, A.; Karasulu, B.; Verheijen, M. A.; Barcones, B.; Macco, B.; Mackus, A. J. M.; Kessels, W. M. M. E.; Roozeboom, F. Area-Selective Atomic Layer Deposition of  $\text{ZnO}$  by Area Activation Using Electron Beam-Induced Deposition. *Chem. Mater.* **2019**, *31*, 1250–1257.

(17) Mamel, A.; Kuang, Y.; Aghaee, M.; Ande, C. K.; Karasulu, B.; Creatore, M.; Mackus, A. J. M.; Kessels, W. M. M.; Roozeboom, F. Area-Selective Atomic Layer Deposition of  $\text{In}_2\text{O}_3:\text{H}$  Using a  $\mu$ -Plasma Printer for Local Area Activation. *Chem. Mater.* **2017**, *29*, 921–925.

(18) Färm, E.; Lindroos, S.; Ritala, M.; Leskelä, M. Microcontact Printed RuOx Film as an Activation Layer for Selective-Area Atomic Layer Deposition of Ruthenium. *Chem. Mater.* **2012**, *24*, 275–278.

(19) Mackus, A. J. M.; Mulders, J. J. L.; van de Sanden, M. C. M.; Kessels, W. M. M. Local deposition of high-purity Pt nanostructures by combining electron beam induced deposition and atomic layer deposition. *J. Appl. Phys.* **2010**, *107*, 116102.

(20) Chaukulkar, R. P.; Agarwal, S. Atomic layer deposition of titanium dioxide using titanium tetrachloride and titanium tetraisopropoxide as precursors. *J. Vac. Sci. Technol., A* **2013**, *31*, 031509.

(21) Anderson, V. R.; Cavanagh, A. S.; Abdulgatov, A. I.; Gibbs, Z. M.; George, S. M. Waterless  $\text{TiO}_2$  atomic layer deposition using titanium tetrachloride and titanium tetraisopropoxide. *J. Vac. Sci. Technol., A* **2014**, *32*, 01A114.

(22) Ramos, K. B.; Clavel, G.; Marichy, C.; Cabrera, W.; Pinna, N.; Chabal, Y. J. In Situ Infrared Spectroscopic Study of Atomic Layer-Deposited TiO<sub>2</sub> Thin Films by Nonaqueous Routes. *Chem. Mater.* **2013**, *25*, 1706–1712.

(23) McGahay, V. Porous Dielectrics in Microelectronic Wiring Applications. *Materials* **2010**, *3*, 536–562.

(24) Grill, A. Plasma enhanced chemical vapor deposited SiCOH dielectrics: from low-k to extreme low-k interconnect materials. *J. Appl. Phys.* **2003**, *93*, 1785.

(25) Edelstein, D. C.; Gates, S. M.; Grill, A.; Lane, M.; Miller, R. D.; Neunmayer, D. A.; Nguyen, S. V. SiCOH dielectric material with improved toughness and improved Si-C bonding, semiconductor device containing the same, and method to make the same. U.S. Patent 20,050,194,619 A1, 2005.

(26) Canaperi, D. F.; Nguyen, S. V.; Priyadarshini, D.; Shobha, H. K. Advanced ultra low k SiCOH dielectrics prepared by built-in engineered pore size and bonding structured with cyclic organosilicon precursors. U.S. Patent 9,449,810 B2, 2014.

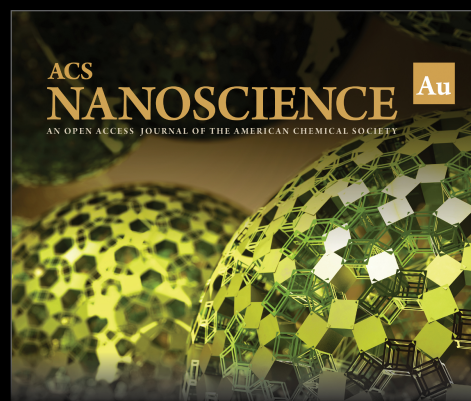
(27) Triyoso, D. H.; Hegde, R. I.; Zollner, S.; Ramon, M. E.; Kalpat, S.; Gregory, R.; Wang, X.-D.; Jiang, J.; Raymond, M.; Rai, R.; Werho, D.; Roan, D.; White, B. E., Jr.; Tobin, P. J. Impact of titanium addition on film characteristics of HfO<sub>2</sub> gate dielectrics deposited by atomic layer deposition. *J. Appl. Phys.* **2005**, *98*, 054104.

(28) Triyoso, D. H.; Hegde, R. I.; Wang, X.-D.; Stoker, M. W.; Rai, R.; Ramon, M. E.; White, B. E., Jr.; Tobin, P. J. Characteristics of Mixed Oxides and Nanolaminates of Atomic Layer Deposited HfO<sub>2</sub>-TiO<sub>2</sub> gate Dielectrics. *J. Electrochem. Soc.* **2006**, *153*, G834–G839.

(29) Sasaki, T.; Ebina, Y.; Kitami, Y.; Watanabe, M.; Oikawa, T. Two-Dimensional Diffraction of Molecular Nanosheet Crystallites of Titanium Oxide. *J. Phys. Chem. B* **2001**, *105*, 6116–6121.

(30) Shchukarev, A.; Korolkov, D. XPS Study of Group IA Carbonates. *Cent. Eur. Sci. J.* **2004**, *2*, 347–362.

(31) Rammula, R.; Aarik, J.; Mändar, H.; Ritslaid, P.; Sammelselg, V. Atomic layer deposition of HfO<sub>2</sub>: Effect of structure development on growth rate, morphology and optical properties of thin films. *Appl. Surf. Sci.* **2010**, *257*, 1043–1052.



Editor-in-Chief: **Prof. Shelley D. Minteer**, University of Utah, USA



Deputy Editor:

**Prof. Raymond E. Schaak**

The Pennsylvania State University, USA

**Open for Submissions** 

pubs.acs.org/nanoau

 ACS Publications  
Most Trusted. Most Cited. Most Read.